Materials Chemistry and Physics, Vol. 103, Issue 2-3 (2007) 295-304.

The structural genesis of a complex $(MoVW)_5O_{14}$ oxide during thermal treatments and its redox behavior at elevated temperatures

G.A. Zenkovets, G.N. Kryukova, V.Yu. Gavrilov, S.V. Tsybulya, V.A. Anufrienko, T.A. Larina, D. F. Khabibulin, O.B. Lapina, E. Rödel*, A. Trunschke*, T. Ressler*, R. Schlögl*

Boreskov Institute of Catalysis of SB RAS, pr. Lavrentieva 5, 630090 Novosibirsk, Russia

**Fritz-Haber-Institut der MPG, Faradayweg 4-6, 14195 Berlin, Germany*

E-mail: trunschke@fhi-berlin.mpg.de

Abstract

The structural genesis of a $Mo_{0.68}V_{0.23}W_{0.09}$ oxide with Mo_5O_{14}-like structure has been examined. A precursor prepared by spray-drying of mixed aqueous metal salt solutions was calcined in air and subsequently treated in helium at different temperatures. X-ray diffraction, HRTEM, ^{51}V MAS NMR, ESR, UV/Vis DR spectroscopy and oxygen and hydrogen adsorption measurements have been applied to monitor the preparation procedure. It was found that a structure closely related to that of Mo_5O_{14} already appears at nano-scale level after calcination of the spray-dried precursor in air at 350°C. At this stage, the material comprises of crystalline particles less than 3 nm in size stabilized by an amorphous matrix. Further heating causes nano-structural rearrangements that lead to the formation of the final $Mo_{0.68}V_{0.23}W_{0.09}$ oxide with phase-pure polycrystalline structure. Molybdenum and tungsten ions are hexavalent and coordinated in an octahedral environment. Furthermore, vanadium is present as V^{4+} and V^{5+} ions which partially occupy octahedral sites, whereas highly distorted trigonal pyramidal sites could be accommodated in pentagonal bipyramids of the Mo_5O_{14} structure, however, displaced away from the center. According to the results of H_2 and O_2 adsorption the crystalline ternary oxide does not possess accessible micropores. Oxygen pulses at 450°C and reductive treatment with pure hydrogen at 300°C did not cause noticeable changes of the bulk structure thus indicating a remarkable structural stability of the complex MoVW oxide under redox conditions at elevated temperature.

Keywords

Nanostructures, molybdenum oxide, Mo_5O_{14}, electron microscopy

Introduction

The selective oxidation of acrolein to acrylic acid is catalyzed by mixed oxides basically composed of molybdenum and vanadium. With regard to industrial application the binary system has been modified with a multitude of elements, W and Cu cited as examples [1-4]. Materials with similar basic composition have shown promising performance in partial oxidation and ammoxidation of light alkanes, e.g. propane, as well [5-7]. An assignment of chemical and structural specifics to catalytic properties is based upon sterical interpretation rather than on experimental results of physical and chemical characterization [7]. Recently, Mo-V-W mixed oxides consisting of $(MoVW)_5O_{14}$ as the major phase have been studied in the selective oxidation of various substrates including methanol, propylene and acrolein [8-10]. In contrast to well-crystallized Mo_5O_{14} oxide, which shows poor activity in the oxidation of acrolein, an amorphous material equally composed but pretreated under different conditions exhibits much increased activity. The latter catalyst undergoes further activation in the course of reaction that is accompanied by an increasing crystallization into the Mo_5O_{15}-type structure [10]. This material remains of considerable stability once operated under steady state conditions. These findings express, on the one hand, the relevance of amorphous fractions and highly disordered phases as precursors for effective catalysts in selective oxidation. On the other hand, the function of the catalyst remains far from being understood, especially with respect to structural and sterical details beyond the identification of a "phase" as active component. Based on this experience, we target the reduction of the structural complexity of Mo-V-W mixed oxides, avoiding phenomena of phase co-operation and structural "synergy". By spray-drying a mixture of aqueous metal salt solutions followed by thermal activation in air and helium we synthesized a material containing one single $(MoVW)_5O_{14}$-type phase [11]. The molecular structure comprising of molybdate species linked via vanadyl ions is pre-assembled as a polymeric network already in the mixed precursor solution [12]. In the present paper, the structural transformations were studied occurring during thermal pretreatment of the spray-dried precursor leading to a phase-pure $(MoVW)_5O_{14}$ material. The initial dynamics of the material and its stability under oxidizing and reducing conditions were investigated by XRD, HREM, ^{51}V MAS NMR, ESR, UV/Vis DR spectroscopy and chemisorption measurements. Novel structural peculiarities have been revealed during crystallization of the $(MoVW)_5O_{14}$ phase that are relevant for the understanding of structural arrangements of complex metal oxides belonging to the Mo_5O_{14} structural family.

Experimental

The precursor of the $Mo_{0.68}V_{0.23}W_{0.09}$ oxides was prepared by spray-drying a mixture of aqueous solutions of ammonium heptamolybdate, ammonium metatungstate and vanadyl oxalate. The precursor obtained was calcined at 350^{o}C in air and subsequently heated in flowing He (flow rate 3.6 l/h, heating rate was 6°C/min) at different temperatures in the range between 380 and 450^{0}C. Details of the preparation procedure have been published elsewhere [11].

XRD analysis was carried out in the 5-70 2Θ range with an URD-63 X-ray diffractometer using CuKα radiation scanning continuously (2°/min). *In-situ* XRD experiments were performed on a STOE Bragg-Brentano diffractometer employing a Bühler HDK S1 chamber. The overall heating rate during *in-situ* XRD was 0.77 °C/min. Measurements were conducted under atmospheric pressure in flowing reactants (~ 100 ml/min). Transmission XAS experiments were performed at the V-K edge at beamline E4 at HASYLAB (Hamburg). The average oxidation state of V was determined from the pre-edge peak height.

HRTEM study was performed on JEM-2010 transmission electron microscope (point resolution, 0.14 nm, acceleration potential, 200 kV). Samples for HRTEM analysis were prepared from suspensions of the powder in ethanol. A drop of the ethanol slurry was placed into the holley-carbon film mounted on a copper grid.

To investigate the stability of the crystalline $(MoVW)_5O_{14}$ material towards reductive and oxidative treatments, a sample heated up to 440^{o}C in He and kept for 1 h at this temperature was subjected to oxygen pulses until saturation (volume per pulse 0.5 cm^3). Afterwards, the sample was cooled down to room temperature in He. For the reductive treatment the sample was placed into a flow reactor, heated up to 300^{o}C in He flow, kept at this temperature for 1 h and treated with flowing hydrogen (flow rate 80 cm^3/min) for 2 h. After treatment the material was cooled down to the room temperature in helium.

The ESR spectra were obtained with a Bruker ESR-500 spectrometer with 100 kHz field modulation in the temperature range of 77-300 K; g-factors were determined using DPPH as a standard. The accuracy of the g-factors measurement was not higher than 0.01. The line widths were measured with the accuracy ± 10G.

MAS and static ^{51}V NMR experiments were done using a Bruker AVANCE-400 (9.4 T) spectrometer at a resonance frequency of 105.20 MHz. The MAS experiments were performed with 4 mm and 2.5 mm rotors (Bruker) using single pulse sequence with rf pulse duration of 1 μs (less than π/10) and recycle times from 0.1 to 1 s. The samples were spun at 12 to 35 kHz. The static ^{51}V spectra were measured using Quad-Echo pulse sequence $90x\text{-}\tau\text{-}180°y\text{-}\tau$. The π/12 - pulse was 1.0 μs and τ varied from 50 to 200 μs. The ^{51}V chemical shifts were referenced to $VOCl_3$ as an external standard. The parameters of ^{51}V NMR spectra were determined from MAS and static spectra using the MASSA approach [13]. Simulations of both static and MAS NMR spectra were performed taking into account the second-order quadrupole correction using the NMR5 program described earlier [13-15]. All simulations were performed on the dual PII-400 MHz CPU IBM PC compatible computer running under Linux OS.

UV/Vis diffusion reflectance spectra (UV/Vis DR) were recorded in a range from 11 000 to 54 000 cm^{-1} with a Shimadzu UV-2501 PC spectrometer. The measurements were performed in air at room temperature. The computer processing of the spectra consisted of two steps including subtraction of the background and calculation of the Kubelka-Munk function F (R_∞).

The adsorption isotherms of oxygen and hydrogen were measured with Digisorb-2600 (Micrometrics) at 77.4 K. Before measurements, the samples were evacuated at 350°C for 5 h. Pore volumes have been calculated by comparing the adsorption isotherms of oxygen and hydrogen with standard isotherms [16, 17] and by volumetric methods [18]. The BET specific surface areas have been obtained by using the oxygen adsorption isotherms.

Results and discussion

XRD and HRTEM

Figure 1 shows the XRD patterns of $Mo_{0.68}V_{0.23}W_{0.09}O_x$ after spray-drying and heat treatments at different temperatures in helium. Complementary, the local structure was investigated by HRTEM (Fig. 2). The spray-dried material is x-ray amorphous showing an ambiguous feature between 5 and 15° 2Θ that encompasses the (210) and (310) reflections in the patterns of Mo_5O_{14} [19] (Fig. 1, curve 0) (ICSD 27202). A second broad peak, located at ca. 27.5° 2Θ, could be associated with the (550) reflection of the same structure. This observation is in a full agreement with HRTEM experiments revealing the amorphous nature of the sample, which consists of big aggregates (about 5 μm) (Fig. 2a). Distinctive lattice fringes are not observable. Selected area

electron diffraction pattern (SAED) obtained from the aggregates and given in the inset of Fig. 2a also confirms the amorphous state of the material by showing a broad diffuse ring.

The XRD patterns are changed by calcination of the spray-dried sample at 350°C in air. A broad peak appears at 22° 2Θ that is very close to the position of the (001) reflection of Mo_5O_{14}. Another broad peak is registered at 26.5° 2Θ (Fig. 1, curve 1). Based on the XRD results, the structure seems to be highly imperfect with little order along the basal plane and some regularity along the [001] direction. However, HRTEM visualizes a specific nanostructure of the particles. The aggregates, which are of the same dimensions as the aggregates in the spray-dried sample, comprise of tiny particles of 3 nm and lower in size having lattice fringes equal to 0.38 nm that could correspond to d_{600} spacing of the Mo_5O_{14} structure (ICSD 27202). As evident from Fig. 2b, these species are randomly distributed with respect to each other in the aggregate. The crystalline regions are separated by interface layers characterized by an amorphous or highly distorted structure. The SAED pattern taken from one of these aggregates exhibits two weak rings, d-spacings of those roughly correspond to (600) and (660) reflections of Mo_5O_{14}. Since the size of these nanoparticles is smaller than 3 nm, which is smaller than the critical dimension that can be registered by X-ray powder diffraction, reflections of (h00) and (hk0) types appear very broad in the XRD patterns. Therefore, broadening of the reflections could not be assigned to the amorphous state of the oxide structure but is due to a size effect caused by the specific structural assembling of the material.

When the calcined sample is subsequently heated in helium flow at 380°C, the intensity of the X-ray diffraction peak previously observed at 22° grows and its width decreases. Moreover, a new peak is registered at 25° (Fig. 1, curve 2). Further thermal treatment of the sample at 400°C does not induce noticeable changes, in other words, intensities and shapes of the diffraction peaks are almost not altered (Fig. 1, curve 3).

Temperature rise to 420°C results in the gradual crystallization of the ternary oxide that is reflected in the appearance of additional peaks in the XRD patterns (Fig. 1, curve 4). The broad peak located at 27° 2Θ transforms into a set of sharp reflections corresponding to the characteristic (540), (630), (550) and (640) reflections of Mo_5O_4, thus indicating the growth of coherently scattering domains in the basal plane. The intensity of the (001) peak rises strongly. The particle size calculated on basis of the half width at half maximum (HWHM) of this peak amounts to 15 nm. HREM also gives evidence for slow structural rearrangements of the material inside the ag-

gregates during heat treatment in helium. The thickness of the amorphous interlayer between the tiny crystalline particles decreases while the crystallinity of the particles increases. Simultaneously, the generation of grain boundaries between the nanospecies was clearly observed. At 420°C, the size of the nanoparticles reaches about 20 nm (Fig. 2c). The SAED pattern taken from this material (see inset in Fig. 2c) shows strong diffraction rings and associated diffraction spots that indicate the coalescence of the crystalline particles inside the aggregates.

Further heating at 440°C results in the rapid crystallization of the material and changes in the morphology. The XRD patterns (not shown) are close to patterns observed after heating at 420°C displaying numerous narrow peaks that are assigned to the whole set of reflections characteristic for the regular structure of the Mo_5O_{14} type. The average valence of vanadium in the latter sample was determined by XAS. Least square XANES fit referring to VO_2 and V_2O_5 revealed a 1:1 ratio between V^{4+} and V^{5+}. Significant amounts of molybdenum or tungsten ions in lower oxidation states have not been found. According to HREM, crystals with more than 1000 nm in size have been formed (Fig. 2d). Sharp point reflections observed in SAED pattern of this sample (see insert in Fig. 2d) can be indexed as belonging to the [001] reciprocal zone of a well crystalline phase possessing Mo_5O_{14} like structure [19].

For this material, a transformation of the surface structure during examination under the electron microscope was also established. Fig. 3 shows a sequence of images illustrating the rearrangement of surface and subsurface layers of a single crystal upon irradiation with the electron beam. As evident from these micrographs, disordering of the regular structure occurs rapidly at the surface. The reconstruction proceeds from the surface to the subsurface layers of the crystal and stops when the thickness of the disordered surface layer reaches 10 nm. As it was reported in [20, 21] for NiO, WO_3 and TiO_2, the high-vacuum experimental conditions inside the electron microscope provide a reducing environment that in some cases allows the segregation of metals on the surface of oxides possible due to the release of oxygen from near surface or subsurface layers of the materials.

To study the stability of the $(MoVW)_5O_{14}$ structure, the material pretreated in He at 440°C was exposed to oxidizing and reducing atmosphere at elevated temperature. Surprisingly, XRD patterns of the sample treated with oxygen pulses at 450°C up to full saturation do not differ significantly from the patterns after treatment in hydrogen flow at 300°C. In turn, the two patterns resemble the patterns of the initial sample. Furthermore, the considerable structural stability of the crystalline $(MoVW)_5O_{14}$ material was confirmed by *in-situ* XRD**.** As it becomes evident

from the XRD patterns given in Fig. 4a and b, the structure remains stable up to 500°C under a flow of 20% oxygen in helium. Extension of the lattice parameters results from the temperature increase but no phase transformation of the structure occurs. Beginning from 400°C in the environment of 10% hydrogen in helium, reduction is indicated by the transformation of Mo_5O_{14} into a monoclinic structure related to that known for MoO_2 and WO_2.

Thus, upon thermal activation and change of the oxygen potential as reported so far, X-ray diffraction reveals a substantial structural stability of our $(MoVW)_5O_{14}$ material as found for MoO_3 [22]. This experimental observation appears to be important, since for metastable oxides rapid phase transformation would be expected. On the other hand, it is well known that the Mo_5O_{14} structure can be stabilized by doping with various transition metal elements like tantalum, vanadium, niobium or tungsten [23, 24, 25]. In particular, niobium [26] and tungsten addition results in thermally resistant materials with structures closely related to that of Mo_5O_{14} but diminished tendency towards disproportionation into the stable binary oxides. At the same time, some rearrangement of the oxide structure may occur on the surface or in subsurface layers in almost the same manner as the reconstruction of the $(MoVW)_5O_{14}$ surface observed by *in-situ* HREM in the electron microscope chamber. Compared to the diameter of the micro crystals (about 0.5 µm), the rearranged layer might be rather thin (about 10 nm). Therefore, such structural changes could not be detected by X-ray diffraction. Nevertheless, it seems very likely that temperatures higher than 300°C and/or longer exposure times in reducing or oxidative atmosphere would lead to phase transformations or total destruction of the $(MoVW)_5O_{14}$ structure.

Thus, here we may conclude that a structural motif closely related to the Mo_5O_{14} structure is formed by calcination of the spray-dried precursor in air at 350°C. The calcined material consists of nanosized $(MoVW)_5O_{14}$ crystals stabilized by an amorphous matrix. Further structural genesis happens via nanostructural assembling by heating in He. The process leads to the formation of a crystalline material consisting of a single phase of the Mo_5O_{14} type. With respect to the phase structure, the final product appears to be fairly stable under oxidizing and reducing conditions.

UV/Vis DR spectroscopy

Fig. 5 compares the UV/Vis DR spectrum of the spray-dried precursor with the spectra of ammonium heptamolybdate (AHM), vanadyl oxalate, ammonium metatungstate (AMT) and the mechanical mixture of these components with the same elemental ratio as in the precursor. The

spectrum of the spray-dried precursor differs significantly from that of the mechanical mixture. It shows absorption bands in the d-d transition region of d^1 vanadyl ions at 12300 cm^{-1} and 14600 cm^{-1} [27]. These bands are shifted to lower wavelengths compared to the spectra of pure vanadyl oxalate as well as the mechanical mixture. In the spectra of the reference materials the corresponding d - d transitions have been observed at 13700 cm^{-1} (b_2-e*) and 16500 cm^{-1} (b_2-b_1*), respectively. The shift of the bands in the spectrum of the spray-dried precursor indicates rearrangements in the surrounding of the central vanadium atom compared to the initial vanadyl oxalate. Moreover, an additional feature was observed at 19000 cm^{-1} that was absent in the reference spectra. This band cannot be assigned to d - d transitions due to its high extinction. However, it can be attributed to the charge-transfer transition from a p-orbital of a bridging oxygen ligand into a vacant d-orbital of vanadium or molybdenum. A similar characteristic absorption band has been observed previously after mixing aqueous solutions of the three precursor compounds [12]. The band was attributed to the formation of new Mo-O-V bonds developing a polymeric network in solution in which the vanadyl species act as linkers between molybdate species.

As evident from Fig. 6, the spectrum of the spray-dried precursor does not change after thermal treatment at 200°C in air. Higher pretreatment temperatures (250°C and 350°C) lead to a shift of the absorption band at 19000 cm^{-1} to 17000 cm^{-1}, whereas the d-d-transition bands of the VO^{2+} ions were not influenced. TGA experiments on the same sample have shown that NO_x and CO_2 are released at 250°C due to the decomposition of the parent ammonium and oxalate salts [11]. Further, the transformation into the oxide is finished at 350°C, albeit, 3D ordering is not yet observable by XRD. It is likely that the shift in the charge-transfer band position is due to this chemical transformation. When the temperature is raised to 440°C in helium, clear changes occur in the spectrum. Since XRD clearly indicates the formation of a well-crystalline $(MoVW)_5O_{14}$ phase under these conditions, the band at 12300 cm^{-1} could be assigned to a ligand to metal charge-transfer transition or a d-d transition characteristic for the regular Mo_5O_{14}-type structure. The latter spectrum was not influenced by subsequent treatments with oxygen pulses at 450°C or hydrogen flow at 300°C indicating that the electronic structure of the material was not changed remarkably. This is in line with the results of the diffraction analysis providing evidence for a high structural stability of $(MoVW)_5O_{14}$ under oxidative and reductive conditions at elevated temperatures.

ESR spectroscopy

The ESR spectrum of the spray-dried sample shown in Fig. 7 (curve 1) exhibits a superposition of two signals, namely, a slightly anisotropic and broad line with $g_{\perp} = 1.96$ and $g_{II} < g_{\perp}$ and a line with hyperfine splitting characterized by the following parameters: $g_{II} = 1.93$, $A_{II} = 200$ G and $g_{\perp} = 1.98$, $A_{\perp} = 77$ G. The width of the first line does not depend on the temperature of measurement. Similar signals were observed for the mixed aqueous solutions of ammonium heptamolybdate and vanadium oxalate during preparation of the solid [12]. The former broad signal was assigned to the presence of associated vanadyl ions, which could be linked by molybdenum forming species like VO^{2+}-O-Mo^{6+}-O-VO^{2+} [12]. The other signal with hyperfine splitting arises from isolated VO^{2+} ions in octahedral environment [28]. Therefore, we can conclude that similar molecular species exist in the starting solution and in the spray-dried material. Cross-linking by Mo-O-V bridges would also be in agreement with the UV/Vis spectroscopic results. Calcination of the spray-dried material at 350°C in air as well as subsequent annealing in He at 380 and 420°C did not change the ESR spectrum noticeably. Finally, the well crystalline $(MoVW)_5O_{14}$ oxide obtained at 440°C in He shows a narrowed signal characteristic for associated vanadyl ions. Moreover, the hyperfine splitting disappeared indicating a homogeneous and well ordered distribution of the associated vanadyl ions across the entire bulk. These observations are in line with the results of XRD and HREM analysis. According to this, $(MoVW)_5O_{14}$ calcined in air at 350°C and subsequently heated in He at temperatures below 420°C consists of small crystalline particles finely divided in a matrix with highly distorted (defect) structure. It seems to be likely that isolated vanadyl ions are stabilized mainly in the vicinity of those defects. Upon raising the temperature up to 440°C in He, extensive crystallization of the material occurs and a ternary oxide with perfect bulk structure is formed. Simultaneously, the signal with hyperfine splitting for isolated vanadyl ions disappeares from the ESR spectrum and the signal responsible for associated vanadyl ions exclusively remains.

^{51}V MAS NMR spectroscopy

^{51}V NMR spectroscopy has been used for characterization of the local structure of V^{5+} sites in the crystalline $(MoVW)_5O_{14}$ oxide. Applying advanced techniques, such as high-field NMR, ultrahigh-speed magic angle spinning (MAS) and satellite transition spectroscopy (SATRAS), solid-state ^{51}V NMR spectroscopy can deliver direct and precise information on the local struc-

ture of vanadium sites, i.e., (i) the number of nonequivalent sites, (ii) coordination numbers, (iii) nature of the atoms in the first coordination sphere, (iv) the distortion of this coordination sphere and (v) the association of polyhedrons [14]. ^{51}V MAS and static NMR spectra of the well crystalline oxide material pretreated at 440°C in He are shown in Figure 8a. The static spectrum represents a broad line with an axial anisotropy. Spinning sidebands are not resolved in the ^{51}V MAS spectrum obtained at 12 kHz and only slightly resolved at 35 kHz. The isotropic chemical shift has been determined from the latter spectrum to be δ_{iso} = -980 ± 50 ppm. Broadening of the spinning sidebands is probably caused by a distortion of the VO_x polyhedrons. At the same time, line broadening may indicate the presence of paramagnetic sites. Basically, the spectrum can be associated with a single type of V^{5+} sites. The ^{51}V NMR parameters obtained from a combined analysis of the MAS and the static spectra are given in Table 1.

In order to determine the coordination of vanadium, the NMR parameters obtained for $(MoVW)_5O_{14}$ were compared with typical values for different coordination spheres, compiled in Table 1 [14]. Note that the NMR parameters determined for $(MoVW)_5O_{14}$ do not coincide with any of the common local environments of the vanadium nucleus reported so far. The small value of η_σ *(< 0.6)* and the large value of $\delta_\perp$ (-470 ppm) indicate a trigonal pyramidal arrangement of the oxygen ligands in the first coordination sphere. However, the large anisotropy value ($\delta_\sigma \approx$ 1000 ppm), atypical for regular trigonal pyramidal coordination, might be caused by strong distortion. Partial reduction of the sample, as well as oxidation influences mainly the intensities of the spectra, but does not lead to changes in the coordination of vanadium sites as evident from spectra shown in Fig. 8b and c.

Texture studies

Adsorption isotherms of oxygen and hydrogen are widely used for characterization of the microporous structure of adsorbents and catalysts, e.g. zeolites [29]. We may apply this approach to our complex metal oxide. The structure of the ternary MoVW oxide is closely related to that of Mo_5O_{14} which shows a complex network of MO_6 octahedra forming slabs that are stacked in such a way that channels are formed [8, 19]. The structure of pure Mo_5O_{14} may tolerate additional ions and it has been discussed in the literature that Mo, V or Te ions may partially occupy these channels [30, 31]. Considering the Mo-O distances determined by XRD, the channel diameters of Mo_5O_{14} should be close to 0.5-0.6 nm. We used adsorption isotherms of oxygen and

molecular hydrogen to determine the diameter and the volume of micropores and/or ultramicropores in the crystalline $(MoVW)_5O_{14}$ oxide. The application of these molecules ensures a quantitative coverage of the micro- and ultramicropore volume, since the kinetic diameters of the oxygen and hydrogen molecules are equal to 0.346 and 0.289 nm, respectively [32].

Fig. 9a, b show adsorption isotherms of oxygen and hydrogen on the sample calcined in air at 350°C and on the sample subsequently treated in He at 440°C, respectively. Calculated specific surface areas and pore volumes are given in Table 2. This table illustrates that the specific surface area strongly decrease after heating of the sample in He. At the same time, the volume of the micropores (0.34-0.5 nm in diameter) accessible to oxygen and hydrogen molecules is very small, and these values are comparable with the accuracy of the adsorption measurements. The volume of ultramicropores (0.29-0.35 nm) was calculated to be virtually zero. The results obtained indicate that the two samples do not possess micropores accessible to the oxygen and hydrogen molecules, and we may suggest that there is a lack of empty channels in the structure of the precursor as well as in the well crystalline $(MoVW)_5O_{14}$ material.

Discussion

Thus, our results provide evidence for the complexity of the structural genesis of ternary MoVW oxides. It proceeds from an amorphous solid precursor through assembling of nanosized crystallites up to a final well-crystalline compound. We would like to stress that the transformation of the oxide precursor from a nano-structural state into a regular structure occurs in a fairly narrow temperature interval. This implicates that the conditions of the thermal treatment play a key role in the formation of a Mo_5O_{14} type phase. The latter can be described as a network, built up of MoO_6 octahedrons and MoO_7 pentagonal bipyramids mutually connected by sharing corners and edges. For reasons of stoichiometry, 40% and of the metal cations in the Mo_5O_{14} structure are occupied by M^{5+} ions. Molybdenum can be partially substituted by vanadium or tungsten atoms in more complex oxides. The localization of these heteroatoms in the Mo_5O_{14} structure remains an open question. Though the structure of the complex $(MoVW)_5O_{14}$ compound has not been determined yet, we may provide some suggestions concerning the distribution of the doping ions in the oxide structures. In accordance with XAS, isolated Mo^{5+} ions have not been observed by ESR spectroscopy. Instead of that, V^{4+} ions have been found in octahedral coordination characteristic for vanadyl ions. Since the structure of Mo_5O_{14} is based on slabs of octahedrons occupied by Mo ions, these positions might be, therefore, partially occupied by V^{4+} ions.

At the same time, NMR spectroscopy deliveres certain hints on the presence of V^{5+} ions in an uncommon, maybe highly distorted trigonal pyramidal coordination. We may speculate that these ions substitute Mo^{5+} ions in pentagonal bipyramidal sites [9]. On the other hand, Millet [33] claimed that Sb^{5+} ions are localized in the open channels of a MoVSb oxide that crystallizes into two different phases closely related to that of Mo_5O_{14}. Note that analogies exist in the preferred coordination of Sb^{5+} and V^{5+} ions. Concerning W^{6+}, we suppose that these ions randomly substitute Mo^{6+} ions in the octahedral coordinated sites of the Mo_5O_{14} framework. However, also in this case, we cannot exclude an occupation of the channels. Adsorption data can be regarded as a confirmation of the above suppositions, since a lack of empty channels in the structure of the complex ternary oxide is indicated.

In this paper, we studied the structural stability of $(MVW)_5O_{14}$ upon redox treatments (300^oC in H_2 and O_2 pulses at 450^oC, respectively). These conditions are even more rigid than the reaction conditions usually applied in acrolein oxidation into acrylic acid (reaction mixture: 4% C_3H_4O, 8% O_2, 20% H_2O, $T=290^oC$). It appeared that this material possesses a high structural stability at these temperatures since the bulk structure of the particles does not change. Simultaneously, some structural alterations may occur on the surface or in near surface layers after exposing the crystalline sample to oxygen and/or hydrogen.

Catalytic properties of Mo-based catalysts in different reactions of mild oxidation have been studied extensively for many years. However, the origin of the catalytic activity remains unclear owing to the multiphase character of the systems. Mestl and co-authors [8-10] reported that Mo_5O_{14}-like structures could play an essential role as active phase among other Mo-containing oxides. Recently, we synthesized phase-pure crystalline $(MoVW)_5O_{14}$ and found that this catalyst shows remarkable high selectivity but poor activity in the oxidation of acrolein to acrylic acid [11]. The reason for such a behavior was not clearly understood since several parameters such as chemical composition, crystallite size and modified surface structure may influence the reactivity. In this paper, we show that the structural genesis of this material proceeds through nanostructural assembling of very small oxide particles stabilized in an amorphous matrix. These species serve as nuclei of the $Mo_{0.68}V_{0.23}W_{0.09}$ oxide phase. Upon annealing in helium, gradual coalescence of these building blocks takes place. The microstructure is preserved up to a relative high temperature, between 400 and 440°C the nanocrystalline arrangement of the material changes abruptly and phase-pure $(MoVW)_5O_{14}$ crystals of several micrometers in size are formed.

Beyond the central conclusion on the nanostructural character of the oxide genesis, the second principal point of this study is that the internal structure of these building blocks resembles that of the Mo_5O_{14}-type phase already after calcination in air at 350°C. Thus, choosing proper preparation conditions, we may control three important parameters, namely, particle size, chemical composition and structural disorder of the synthesized material. Future experiments should address the catalytic testing of complex MoVW oxides characterized by different microstructure. Studies on the catalytic behavior of specifically arranged structures may offer significant contributions to the current controversy about the origin of catalytic activity of Mo-based catalysts.

Conclusions

In this paper, the structural genesis of a phase-pure $(MoVW)_5O_{14}$ oxide prepared by spray-drying of aqueous metal salt solutions followed by a two-step thermal treatment in air and helium were investigated using *ex-situ* and *in-situ* XRD and TEM, as well as by hydrogen and oxygen adsorption. Changes in the oxidation state of the metal ions were studied by ESR, ^{51}V NMR and UV/Vis DR spectroscopy. It was found that heating of the spray-dried material in air at 350°C leads to the gradual crystallization of $Mo_{0.68}V_{0.23}W_{0.09}$ oxide nanoparticles with a structure closely related to Mo_5O_{14}. These structural building blocks are embedded in an amorphous or highly disordered matrix. With increasing temperature in helium, the separate particles are subjected to increasing coalescence up to the final formation of large MoVW oxide crystallites with perfect crystal structure. Molybdenum and tungsten are present as hexavalent ions. It was established that V^{4+} ions appear in octahedral coordination, while V^{5+} ions may be arranged in the pentagonal bipyramids in a highly distorted manner. According to the results of O_2 and H_2 adsorption measurements, the highly crystalline ternary oxide does not possess accessible ultramicropores. Oxidizing and reducing treatments of the complex oxide at relatively high temperatures do not lead to significant structural changes thus indicating a remarkable structural stability of the material under redox conditions.

References

1. A.N. Kurtz, R.W. Cunningdam, A.W. Naumann (Union Carbide Co.), US Patent, 4111983, 1978.
2. T. Kawajiri, S. Uchida, H. Hironaka (Nippon Shokubai Kagaku), EP 427 508 A1, 1991.
3. A. Tenten, F.-G. Martin, H. Hibst, L. Marosi, V. Kohl (BASF AG), EP 668104 B1, 1995.
4. T.V. Andrushkevich, *Catal. Rev.-Sci. Eng*. 35 (1993) 213.
5. M.M. Lin, *Appl. Catal. A* 250 **(**2003) 287.
6. D. Vitry, J. L. Dubois, W. Ueda, *J. Molec. Catal*. A 220 (2004) 67.
7. R. K. Grasselli, *Catal. Today* 99 (2005) 23.
8. G. Mestl, Ch. Linsmeier, R. Gottschall, M. Dieterle, J. Find, D. Herein, J. Jäger, Y. Uchida, S. Schloegl, *J. Molec. Catal. A* 162 (2000) 455.
9. M. Dieterle, G. Mestl, J. Jäger, Y. Uchida, R. Schloegl, *J. Molec. Catal*. A 174 (2001) 169.
10. O. Ovsitser, Y. Uchida, G. Mest, G. Weinberg, A. Blume, J. Jäger, M. Dieterle, H. Hibst, R. Schloegl, *J. Molec. Catal. A* 185 (2002) 291.
11. S. Knobl, G.A. Zenkovets, G.N. Kryukova, O. Ovsitser, D. Niemeyer, R. Schloegl, G. Mestl, *J. Catal*. 215 (2003) 177.
12. S. Knobl, G.A. Zenkovets, G.N. Kryukova, R.I. Maksimovskaya, T.V. Larina, N.T. Vasenin, V.F. Anufrienko, D. Niemeyer, R. Schloegl, *PCCP* 5 (2003) 5343.
13. A.A. Shubin, O.B. Lapina, V.M. Bondareva, *Chem.Phys.Lett.* 302 (1999) 341.
14. O.B. Lapina, A .A. Shubin, D.F. Khabibulin, V. V. Terskikh, P. R. Bodart, J.-P.Amoureux, *Catal.Today* 78 (2003) 91.
15. A. A. Shubin, O. B. Lapina, E. Bosch, H. Knozinger, *J. Phys. Chem.* 103 (1999) 3138.
16. A.P. Karnaukhov, V.B. Fenelonov, V. Yu. Gavrilov, *J. Pure & Appl. Chem*. 61 (1989) 1913.
17. V.Yu. Gavrilov, *Kinet. Katal*. 35 (1994) 397.
18. V. Yu. Gavrilov, *Kinet. Katal*. 36 (1995) 580.
19. L. Kihlborg, *Ark. Kem*. 21 (1963) 427; *Acta Chem. Scand*. 23 (1969) 1834.
20. M. Buckett, L.D. Marks, *Surf. Sci*. 232 (1990) 353.
21. R. Ai, H. J. Fan, L.D. Marks, *Surf. Sci. Lett*. 247 (1992) L559.
22. T. Ressler, O. Timpe, T. Neisius, J. Find, G. Mestl, M. Dieterle, R. Schlogl, *Journal of Catalysis* 191 (2000) 75.

23. N. Yamazoe, L. Kihlborg, *Acta Cryst*. B31 (1975) 1666.
24. T. Ekström, *Acta Chem. Scand*. 26 (1972) 1827.
25. T. Ekström, M. Nygren, *Acta Chem. Scand*. 26 (1972) 1836.
26. P. Afanasiev, *J. Phys. Chem. B* 109 (2005) 18293.
27. L. Ballhausen, H.B. Grey, *Inorg. Chem*. 1 (1962) 111.
28. M.V. Paganini, L. Dall'Aqua, E. Giamello, L. Lietti, P. Forzatti, G. Busca, *J. Catal*. 166 (1997) 195.
29. *Catalysis: an Integrated Approach (Studies in Surface Science and Catalysis)*, Ed. P.A. van Santen, P.W.N.M. van Leuwen, J.A. Moulijn, B.A. Averill, Elsevier, Amsterdam, Lausanna, New York, Oxford, Shannon, Singapore, Torronto, 1999, v.123.
30. M. M. Millet, H. Roussel, A. Pigamo, J. L. Dubois, J. C. Jumas, *App. Cat. A* 232 (2002) 77.
31. R. K. Grasselli, J. D. Burrington, D. J. Buttrey, P. DeSanto Jr, C. G. Lugmair, A. F. Volpe, T. Weingand, *Top. Catal*. 23 (2003) 5.
32. *Characterization of Catalysts*, ed. J.M. Thomas, R.M. Lambert, John Willey&Sons, Chichester, New York, Brisbane, Torronto, 1980.
33. J.M.M. Millet, M. Baca, A. Pigamo, D. Vitry, W. Ueda, J.L. Dubois, *Appl. Catal. A* 244 (2003) 359.

Table 1

Experimentally obtained ^{51}V NMR parameters (quadrupole tensor parameter (C_Q) [a], chemical shift tensor parameters (δ_σ, η_σ, δ_{iso})[b]) compared to reference parameters[14].

		δ_σ, ppm	η_σ	$\delta_\perp$, ppm	C_Q, MHz
$(MoVW)_5O_{14}$ pretreated at 440°C in He		1000±50	0.6	-470± 20	
Classification of reference parameters according to [14]					
Coordination					
Tetrahedral					
	Vanadium in regular tetrahedral oxygen environment, Q^0 type	< 100	0 - 1		1 - 6
	Vanadium in slightly distorted tetrahedral sites with the adjacent tetrahedra sharing one common oxygen atom, Q^1 type	100 – 200	0.1 – 0.9		2.5 - 10
	Vanadium in strongly distorted tetrahedral sites with adjacent tetrahedra sharing two common oxygen atoms, Q^2 type	200 – 500	0.6 – 0.8		2 - 7
Pyramidal		>200	<0.6		
	Tetragonal bipyramidal	200 – 500	0 – 0.6	-200– 400	4 - 8
	Tetragonal pyramidal	400-500	0 – 0.6	-200– 400	1 - 4
	Trigonal pyramidal	200 – 500	0 – 0.6	-400– 600	1 - 4
	Trigonal bipyramidal or distorted octahedral	<500	0 – 0.1	-200– 350	0 - 3

[a] C_Q - quadrupolar constant, $C_Q = e^2qQ/h$.

[b] The eigenvalues of chemical shift tensor (CS-tensor) are expressed by δ_σ- chemical shift anisotropy, η_σ - chemical shift asymmetry parameter and $\delta_\perp = 1/2(\delta_1 + \delta_2)$, δ_i—components of CS-tensor. ($\delta_1 = -1/2\delta_\sigma(-1 - \eta_\sigma) + \delta_{iso}$; $\delta_2 = -1/2\delta_\sigma(-1 + \eta_\sigma) + \delta_{iso}$; $\delta_3 = -\delta_\sigma + \delta_{iso}$)

Table 2. Microporous structure of $(MoVW)_5O_{14}$

	Oxygen adsorption isotherm		Hydrogen adsorption isotherm	
Pretreatment	S_{BET}, m^2/g	V_μ**, cm^3/g	V_μ, cm^3/g	$V_{u\mu}$***, cm^3/g
350°C in air	8.9	≈ 0,0002	0,002	0,0002
350°C in air, 440°C in He	4.7	0	0,001	0

** V_μ , accessible volume of ultramicropores with 0.35-0.5 nm in diameter.

*** $V_{u\mu}$, accessible volume of ultramicropores with 0.29-0.35 nm in diameter.

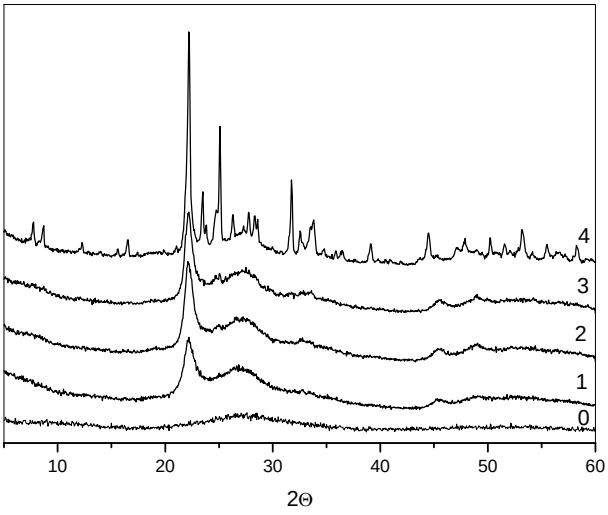

Fig.1. XRD patterns of the spray-dried precursor (0) and of the material after calcination at 350^{o}C in air (1) and subsequent treatment in He flow at 380 (2), 400 (3) and 420^{o}C (4).

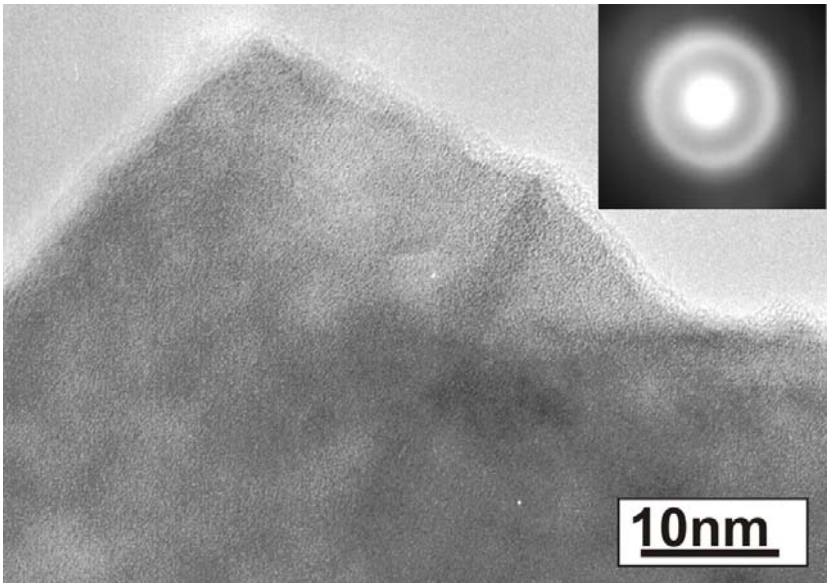

a

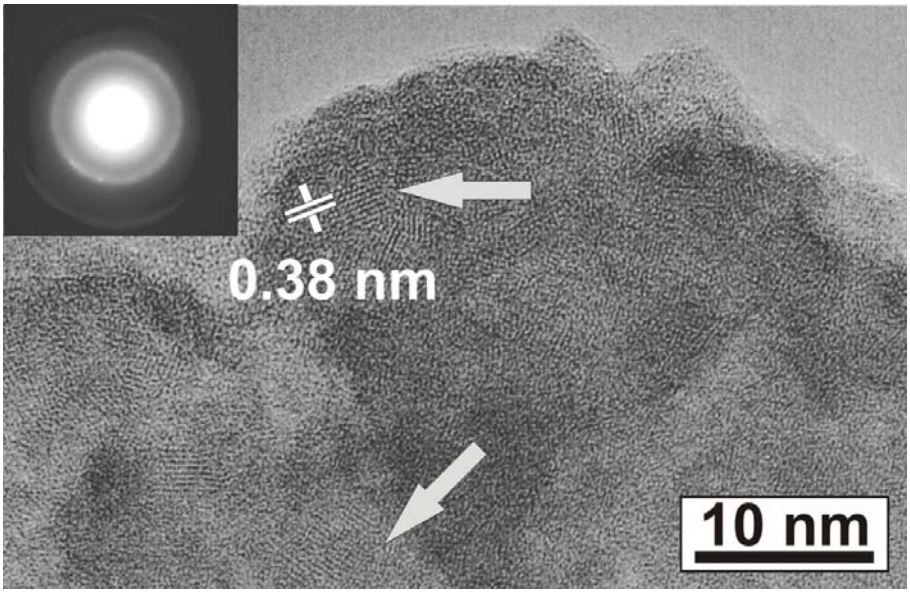

b

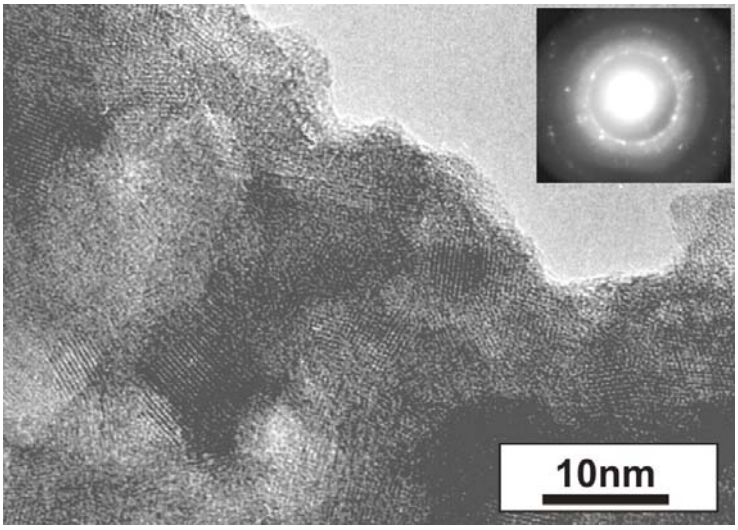

c

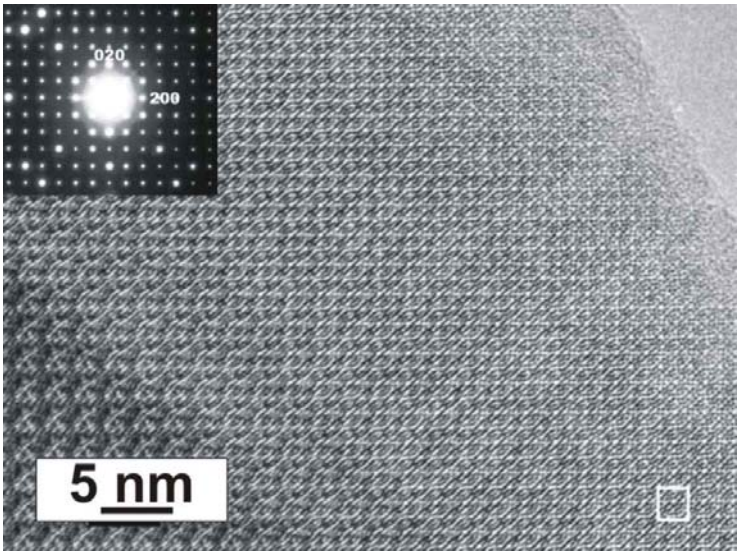

d

Fig. 2. TEM micrographs of the spray-dried precursor (a) and the material calcined in air at 350^{o}C (b) and subsequently treated in He flow at 420 (c) and 440^{o}C (d).

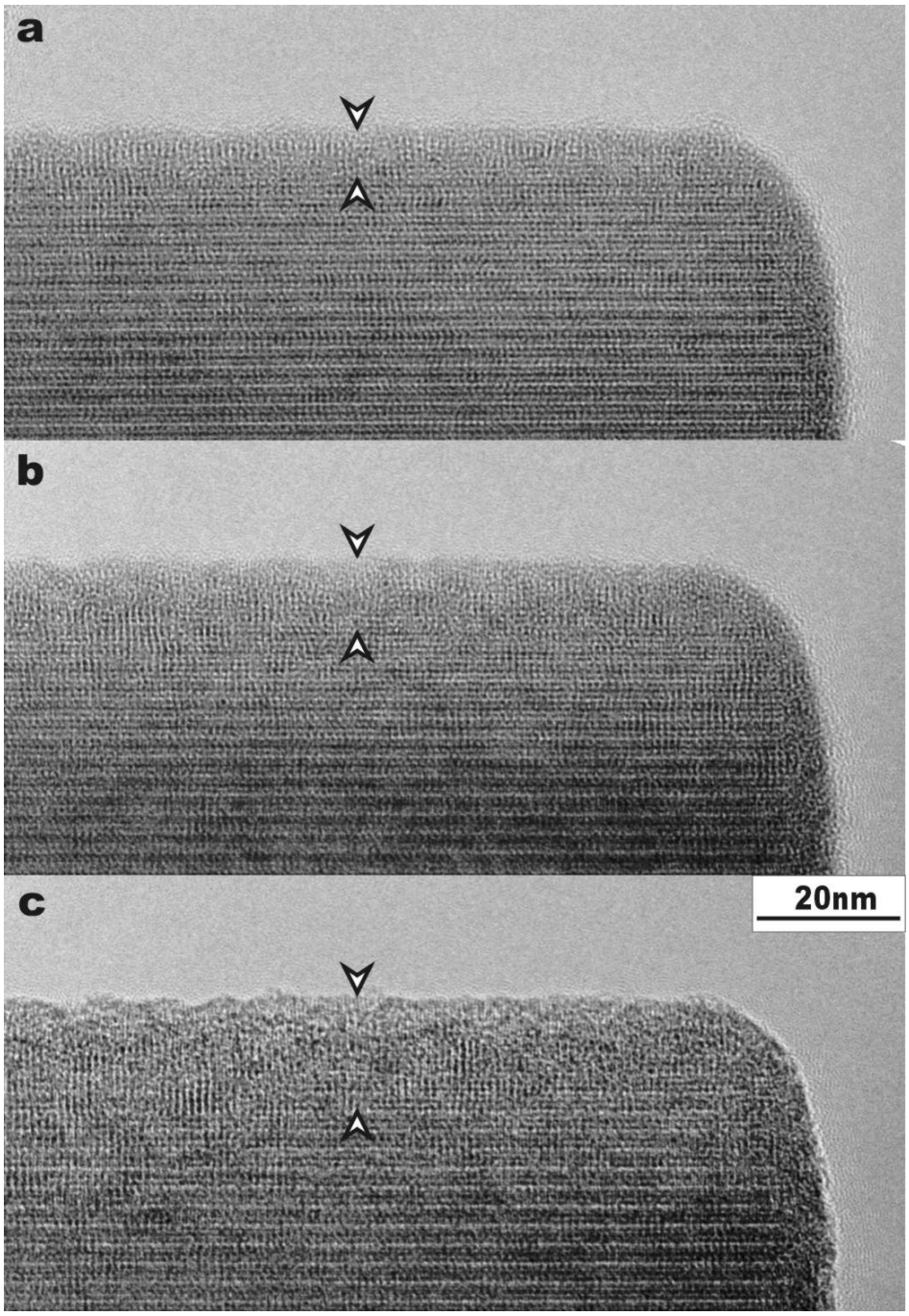

Fig. 3. Sequence of HREM images of the well-crystalline $(MoVW)_5O_{14}$ oxide with Mo_5O_{14} structure after irradiation with the electron beam: a) –5 sec, b) – 20 sec, and c) – 30 sec.

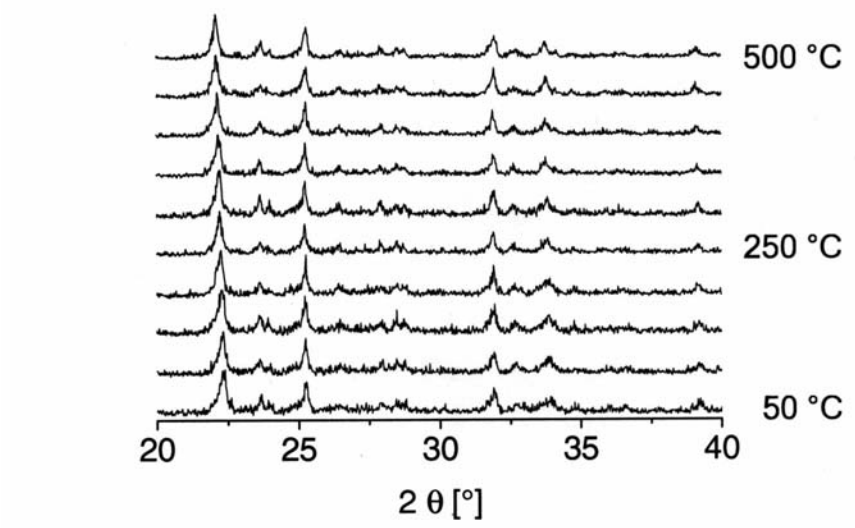

a

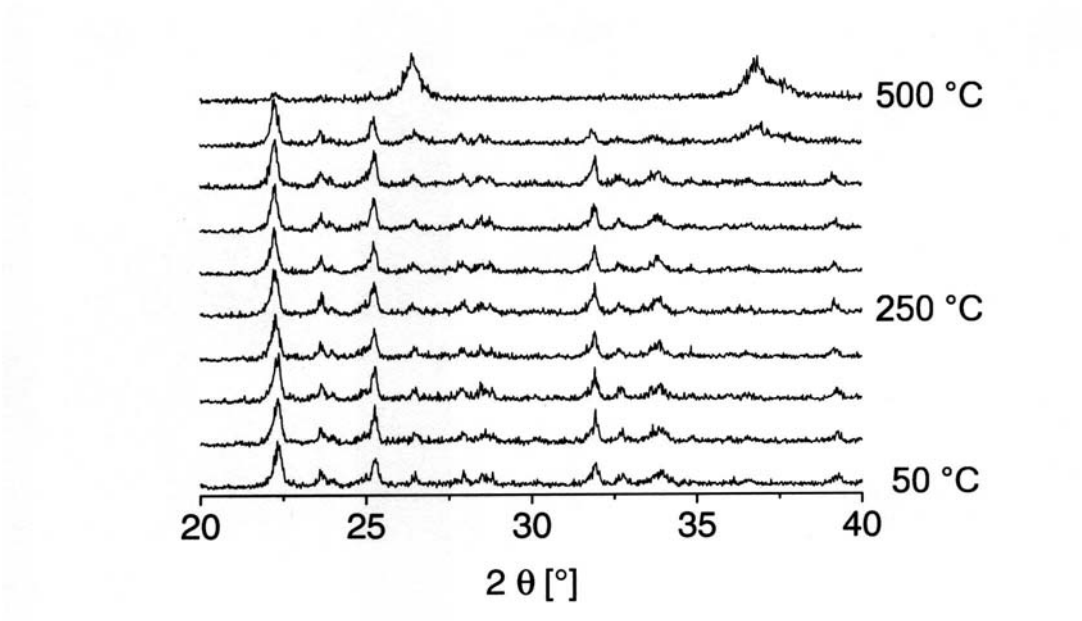

b

Fig. 4. *In-situ*XRD patterns of the crystalline $(MoVW)_5O_{14}$ material registered during heat treatment from ambient temperature to 500^{o}C in the 20% oxygen in He (a) and 10% hydrogen in He (b).

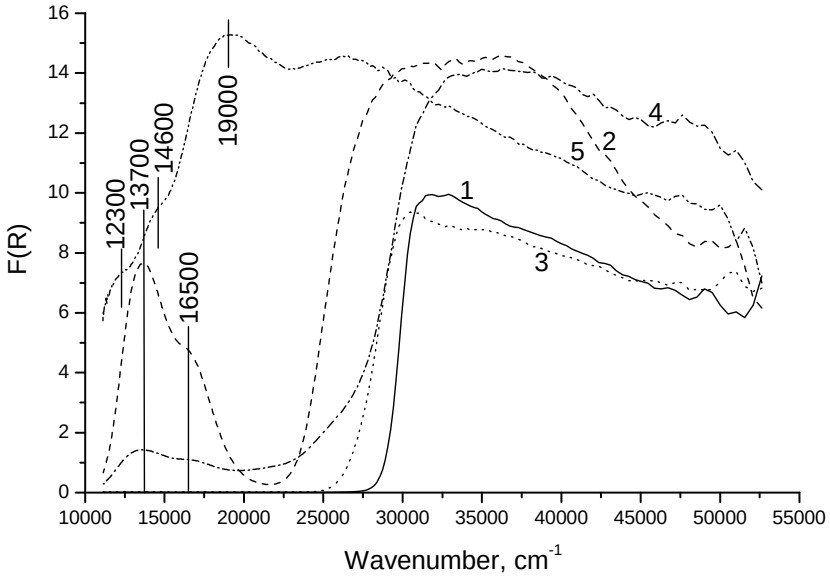

Fig. 5. UV/Vis DR spectra of ammonium heptamolybdate (1), vanadyl oxalate (2), ammonium metatungstate (3), a mechanical mixture of all compounds in molar ratios equal to $Mo_{0.68}V_{0.23}W_{0.09}$ (4) and spray-dried precursor(5).

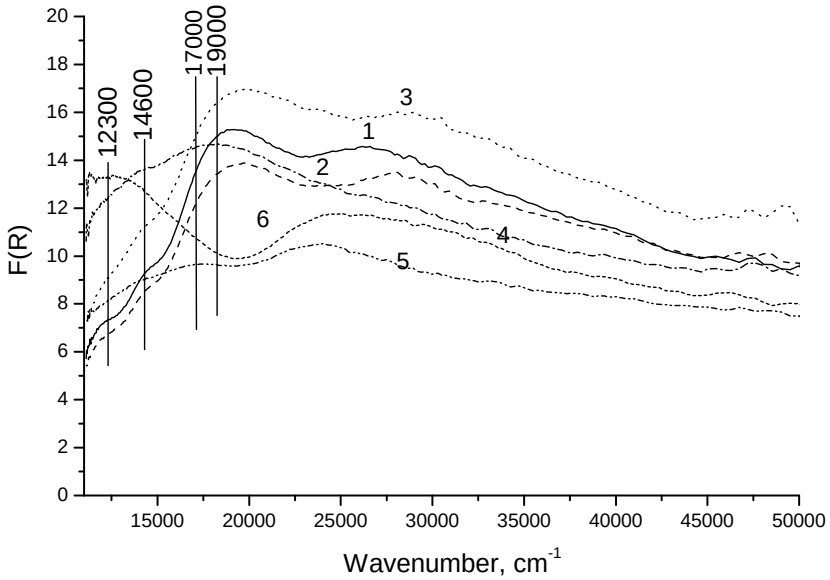

Fig. 6. UV/Vis DR spectra of the spray-dried precursor (1), after heating at 110 (2), 200 (3), 250 (4), 350°C in air (5) and subsequent treatment at 440°C in He (6).

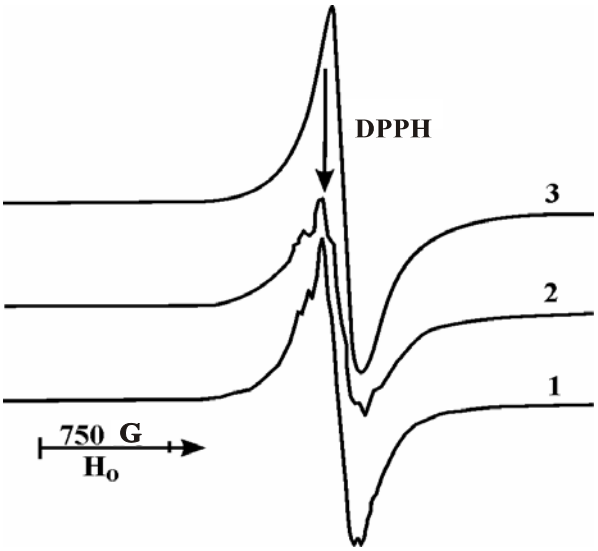

Fig. 7. ESR spectra of the MoVW oxide precursor dried at 110^{o}C in air (1) calcined in air at 350^{o}C (2) and subsequently treated in He flow at 440^{o}C (3).

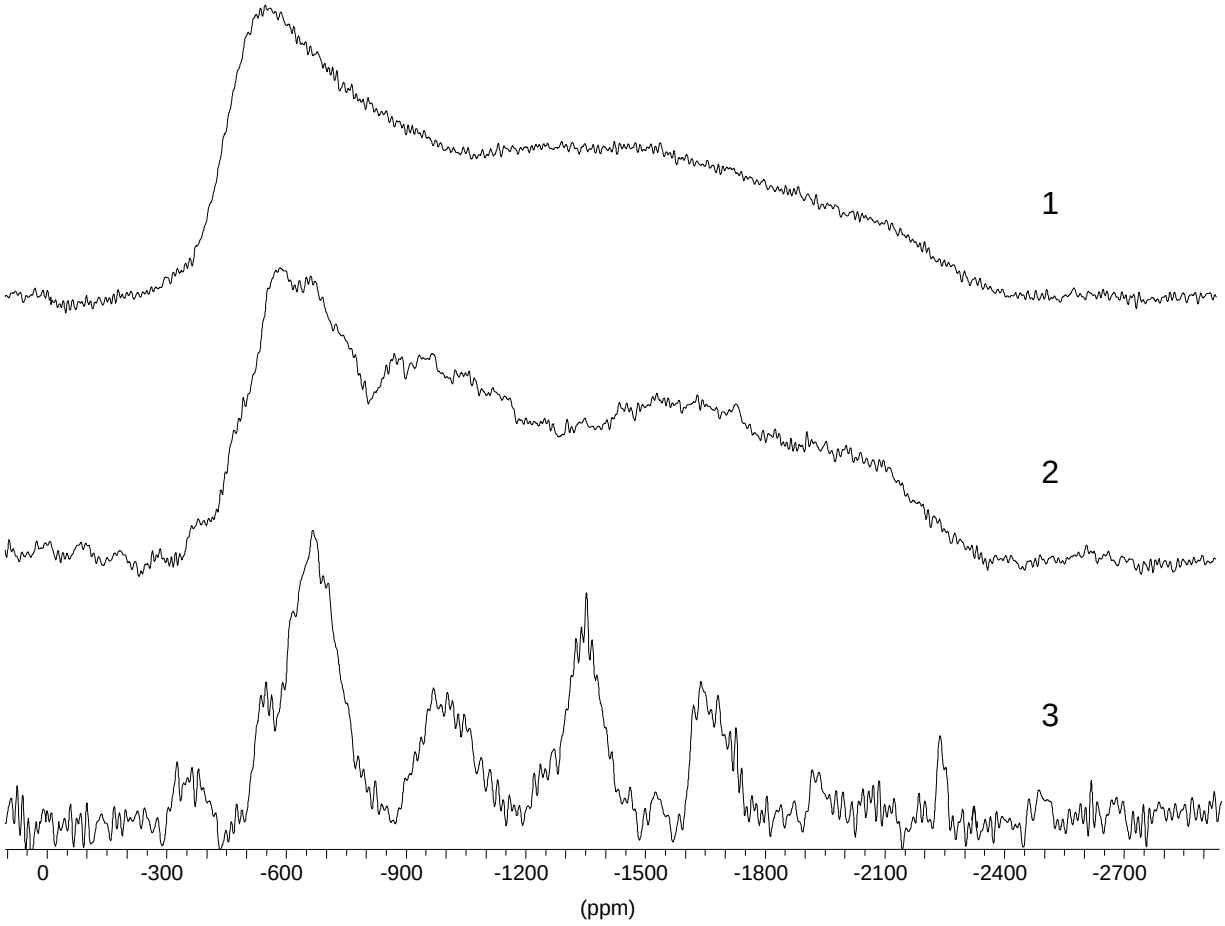

a

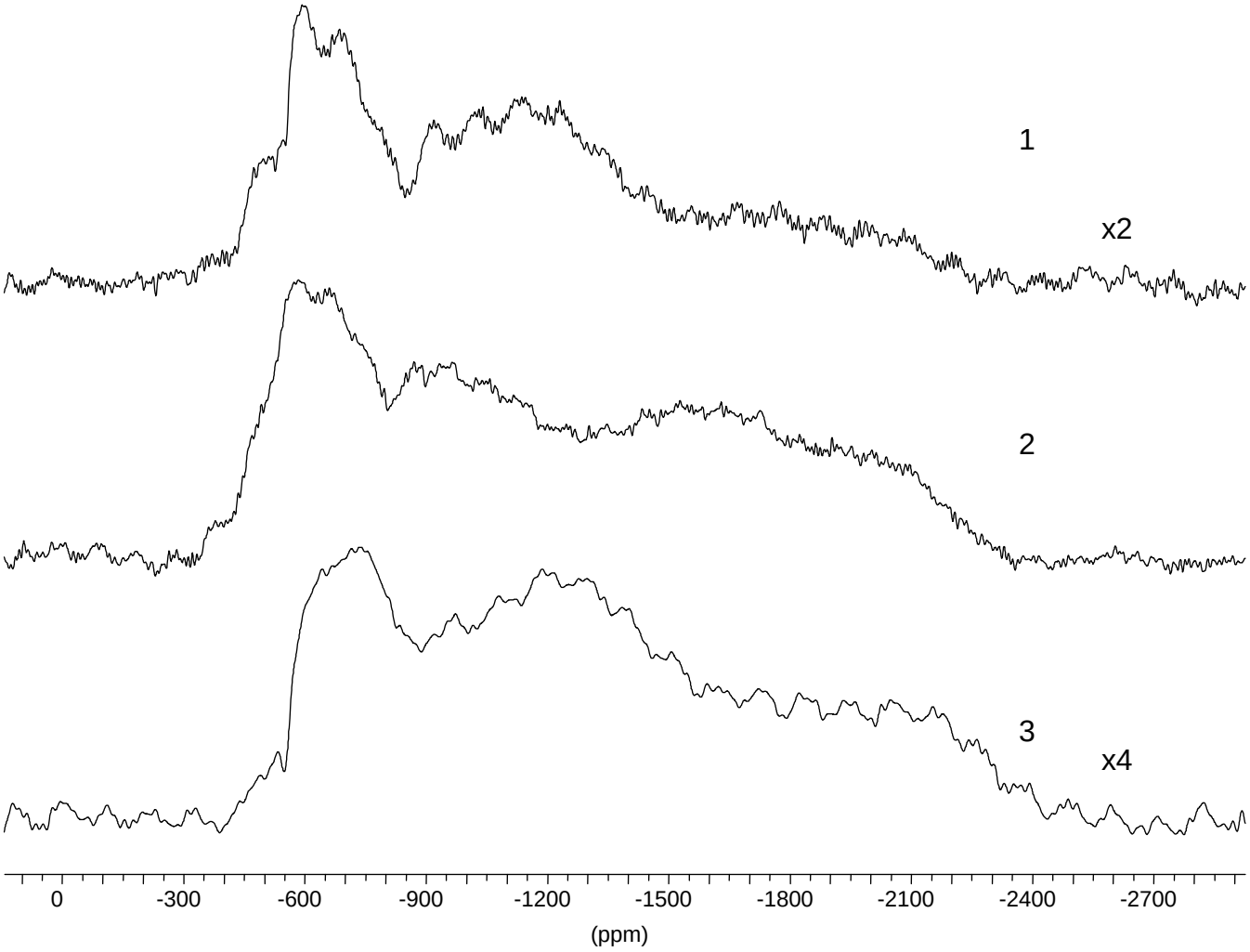

b

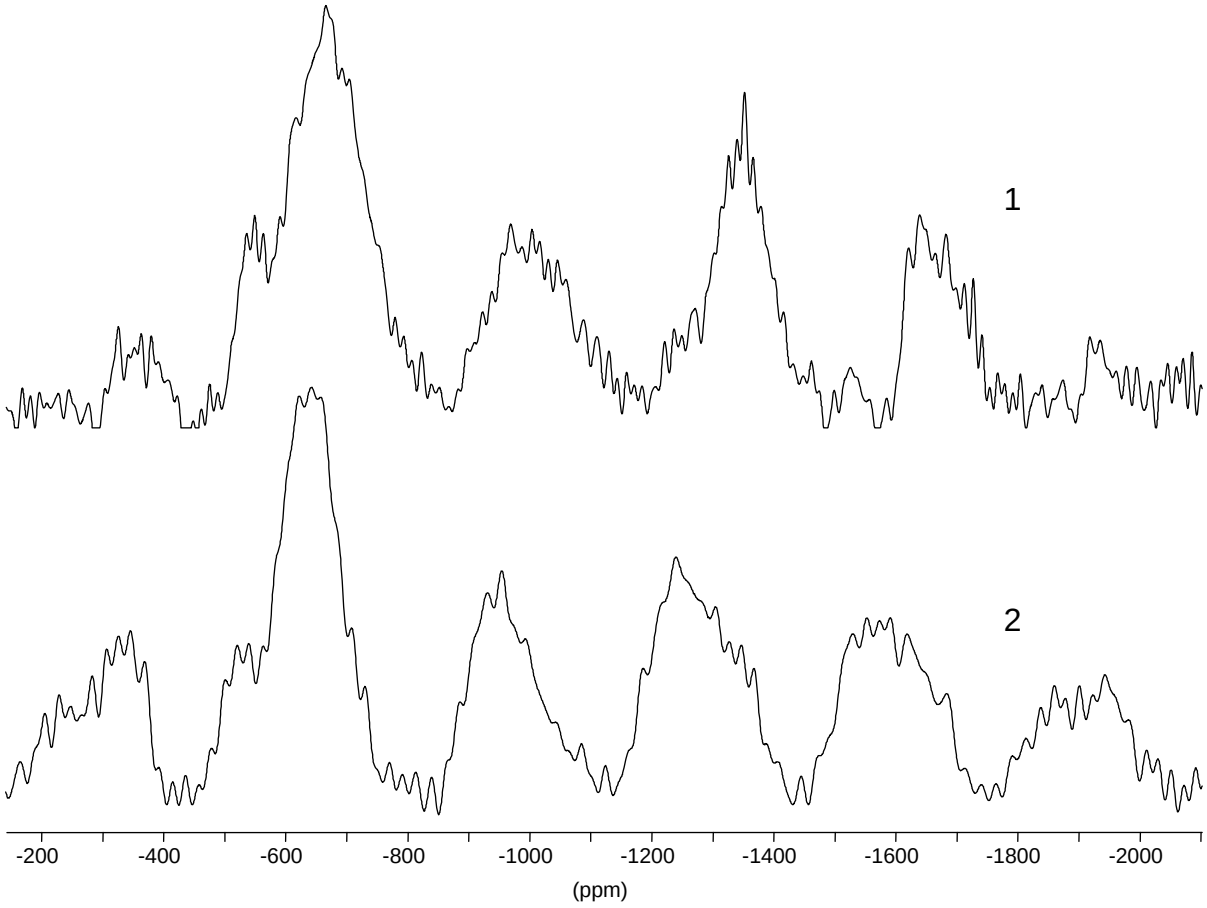

c

Fig. 8. Static (1) and ^{51}V MAS NMR (rotation frequency 12 kHz (2) and rotation frequency 35 kHz (3)) spectra of the single crystalline $(MoVW)_5O_{14}$ oxide (a); ^{51}V MAS NMR spectra of the initial (1), oxidized (2) and reduced (3) well-crystalline $(MoVW)_5O_{14}$ oxide (b, rotation frequency 12 kHz); ^{51}V MAS NMR spectra of the initial (1) and oxidized (2) single crystalline $(VMOW)_5O_{14}$ oxide(c, rotation frequency 35 kHz).

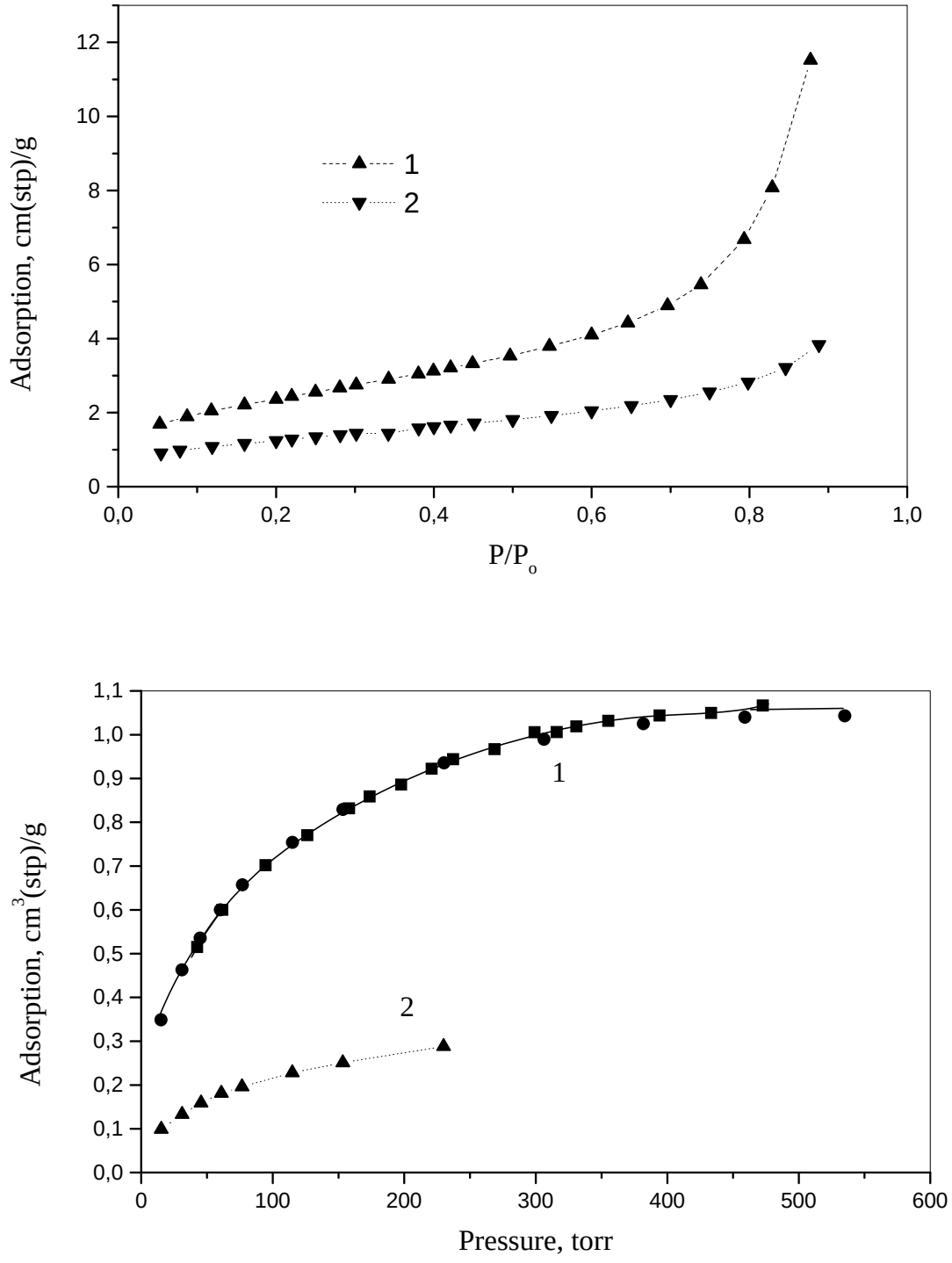

Fig. 9. Adsorption isotherms of oxygen (a) and hydrogen (b) obtained over the samples heated at 350^{o}C in air (1) and subsequently heated at 440^{o}C in He (2).